

This discussion paper is/has been under review for the journal Geoscientific Instrumentation, Methods and Data Systems (GI). Please refer to the corresponding final paper in GI if available.

Interpreting muon radiographic data in a fault zone: possible application to geothermal reservoir detection and monitoring

H. K. M. Tanaka¹ and H. Muraoka²

¹Earthquake Research Institute (ERI), University of Tokyo, 1-1-1 Yayoi, Bunkyo, Tokyo 113-0032, Japan

²North Japan Research Institute for Sustainable Energy (NJRISE), Hirosaki University, 2-1-3 Matsubara, Aomori 030-0813, Japan

Received: 27 August 2012 – Accepted: 8 October 2012 – Published: 24 October 2012

Correspondence to: H. K. M. Tanaka (ht@riken.jp)

Published by Copernicus Publications on behalf of the European Geosciences Union.

Interpreting muon radiographic data in a fault zone

H. K. M. Tanaka and
H. Muraoka

Title Page

Abstract

Introduction

Conclusions

References

Tables

Figures

⏪

⏩

◀

▶

Back

Close

Full Screen / Esc

Printer-friendly Version

Interactive Discussion

Abstract

Rainfall-triggered fluid flow in a mechanical fracture zone associated with a seismic fault has been estimated (Tanaka et al., 2011) using muon radiography by measuring the water position over time in response to rainfall events. In this report, the data taken by Tanaka et al. (2011) are reanalyzed to estimate the porosity distribution as a function of a distance from the fault gauge. The result shows a similar pattern of the porosity distribution as measured by borehole sampling at Nojima fault. There is a low porosity shear zone axis surrounded by porous damaged-areas with density increasing with the distance from the fault gauge. The dynamic muon radiography (Tanaka et al., 2011) provides a new method to delineate both the recharge and discharge zones along the fault segment, an entire hydrothermal circulation system. This might dramatically raise the success rate for drilling of geothermal exploration wells and it might open a new horizon in the geothermal exploration and monitoring.

1 Introduction

Fluid flow through geological scale porous media is of great importance in many areas ranging from civil engineering to geothermal technologies. Such a large scale porous media can be generated in response to lithostatic, tectonic, and thermal stresses and high fluid pressures. The high crack density in the damage zone results in significant pore volume increase; hence improving the water transport properties. Water influx is therefore often dominated by such high-conductivity fracture zones, and thus economically significant geothermal and water supply reservoirs often form in fractured rocks. For example, the fault-hosted geothermal water is captured in fractured rocks within seismic faults. Tunneling through a fault zone can produce a sudden water inflow if it intersects a high-pressure fracture zone. Fracture zones also affect stability, deformation, and fluid flow into underground structures. The penetration of water into fractures can be also hazardous since water-induced pore pressures may increase in response

GID

2, 875–891, 2012

Interpreting muon radiographic data in a fault zone

H. K. M. Tanaka and
H. Muraoka

Title Page

Abstract

Introduction

Conclusions

References

Tables

Figures

⏪

⏩

◀

▶

Back

Close

Full Screen / Esc

Printer-friendly Version

Interactive Discussion



to rainfalls if the fractures are blocked, and as a result, failure may follow. Understanding of the geometrical, porous and permeability structures of fracture zones would improve the design and construction of tunnels, dams, and geothermal plants.

A typical seismic fault structure includes a narrow fine-grained core surrounded by a damage zone of highly fractured rock (Caine and Forster, 1999). A zone that includes the fine grain size in the fault core is called a fault gauge, and expected to have a low porosity. The surrounding damage zone contains a high density of microcracks, and thus is likely to have higher porosity. Conventionally, such a contrast between damage zones and the surrounding rock has been indirectly measured by magnetotelluric imagery (Lockner and Byerlee, 1986), by seismic tomography (Li and Leary, 1990), and more directly by drilling boreholes (Lockner et al., 2009). Although bore hole sampling method provides density contrast along the shaft with a great accuracy, it only provides local information around the drilling hole.

Muon radiography is becoming commonly used imaging technique for geological or plant evaluation and monitoring (e.g. Tanaka et al., 2009). Radiographs are reproducible, and can identify changes in density inside the target volume with fairly high precision and accuracy. However, there are several disadvantages to muon radiography. Firstly, technical limitations include the need for a topographically prominent feature of interest, and there will only be results for the volume located above the detector. This is why a seismic fault on a hill slope made a good study target in the work by Tanaka et al. (2011) (Fig. 1). However, this problem could be solved with borehole/tunnel observations from underground muon detectors (Tanaka and Sannomiya, 2012). Secondly, this technique only resolves the average density distribution along individual muon paths. Therefore, the user must end up making assumptions or interpretations about more localized structure along those muon paths, or must use more than one detector to resolve the three-dimensional density structure.

The muon attenuation is directly proportional to the density of the material with minimal uncertainty due to chemical composition. Muon radiography is therefore provides varying densities inside the geological formations. Among various physical quantities

Interpreting muon radiographic data in a fault zone

H. K. M. Tanaka and
H. Muraoka

Title Page

Abstract

Introduction

Conclusions

References

Tables

Figures



Back

Close

Full Screen / Esc

Printer-friendly Version

Interactive Discussion



measured in the Earth's crust, density plays a special role because it is readily interpreted in terms of porosity of fracture-filling rocks; hence the permeability of the fault zones can be estimated from muon radiography.

Tanaka et al. (2011) measured rain-fall triggered fluid flow in a fracture zone associated with a seismic fault located in Itoigawa-Shizuoka tectonic line with muon radiography. It has been shown that the water front was clearly imaged in response to rainfall events. There, correlations were observed between rainfall events and muon intensities for different depths in the fault zone. The decrease in the muon flux has been interpreted as a result of active fluids trapped inside cracks of the damage zone. After the rain-fall event, the trapped fluid is gradually released from the cracks and as a result the increase in the muon flux was measured. In this work, the data taken by Tanaka et al. (2011) were reanalyzed to estimate the density distribution as a function of a distance from the fault gauge. The method directly measures an average density along the muon path, covering a larger spatial extent. In this report, possible geothermal exploration and monitoring utilizing muon radiography is also discussed.

2 Reanalysis

Itoigawa-Shizuoka Tectonic Line (ISTL) is a major fault that runs from the city of Itoigawa, Niigata Prefecture, through Lake Suwa to the city of Shizuoka in Shizuoka Prefecture. The ISTL is a major geological structure dividing the Japanese mainland into northeastern and southwestern parts. A part of this fault line was discovered by trenching a fault scarp at Fossa Magna Park, the first UNESCO Geopark in Japan, located in the north end of the ISTL. The discovered fault cuts across 16-million-year old basaltic rock. The fault outcrop on a steep hill slope provides an ideal location to study the properties of the fracture (Fig. 1).

The data discussed here were obtained using a detection system with an active area of 3969 cm^2 that was installed 6 m south from the fault outcrop, pointing towards the geologically estimated direction of the fault line (Fig. 1) (Tanaka et al., 2011).

Interpreting muon radiographic data in a fault zone

H. K. M. Tanaka and
H. Muraoka

Title Page

Abstract

Introduction

Conclusions

References

Tables

Figures



Back

Close

Full Screen / Esc

Printer-friendly Version

Interactive Discussion



Interpreting muon radiographic data in a fault zone

H. K. M. Tanaka and
H. Muraoka

Title Page

Abstract

Introduction

Conclusions

References

Tables

Figures

⏪

⏩

◀

▶

Back

Close

Full Screen / Esc

Printer-friendly Version

Interactive Discussion



In order to identify the path of cosmic-ray muons, two segmented detectors were employed as position sensitive detectors (PSDs) in this experiment. The segmented detector consisted of x and y planes. Each plane consisted of an array of scintillator strip. Each scintillator strip with a size of 70-cm length x 7-cm width x 2-cm thickness was composed of a plastic scintillator and a 2-inch photo-multiplier tube. 18 counters were arranged in the x and y planes, and were segmented by a 7-cm square. The path of a muon can be determined by the combination of two signals from the Nos. 1 and 2 segmented detectors. The two segmented detectors were placed at a distance of 70 cm. The triggering requirement for the soft-component rejection analysis is a coincidence within 20 ns of at least two out of 9 counters within the same plane (multiplicity cut analysis method) (Tanaka et al., 2001). Therefore within this framework, the selection criteria for a candidate muon path are follows: there is one signal from each scintillator array plane, the two signals of the counter are detected simultaneously, and the four signals are in a coincidence window. An angle of the incident muon is calculated using the difference between detection positions of two PSD planes.

The angular resolution of the present segmented detection system was evaluated by utilizing a steel block (Tanaka, 2012). The root mean square (RMS) angular resolution of ± 40 mrad defines the ± 24 cm accuracy of the position resolution at the outcrop. However, at a distance of 100 m from the detection system, it becomes ± 4.0 m. The present detection system cannot resolve the density of the fault gauge whose width is 60 cm. The image acquisition was made at a 27-day exposure time. The distance travelled in 2×10^{-8} s is equivalent to that between the detection system and the outcrop, and is much shorter than muon's decay constant of 2.2×10^{-6} s. We therefore neglected the effect of muon decays.

3 Data analysis

Since we expect that cosmic-ray muon flux is azimuthally isotropic within the effective azimuth angle of $-400 \text{ mrad} < \phi < +400 \text{ mrad}$ without a target object, the horizontal

distribution of muons can be used to correct. Figure 2 shows the histogram of the muon events collected in the present experiment. The counts in negative elevation angles mainly consist of the “backward-directed” muons that can be used to confirm the integral muon intensity, its zenith-angular dependence, and the geometrical acceptance of the detection system. The azimuthally symmetric behavior of the counts confirms that the muons are azimuthally isotropic. The raw radiograph was corrected by applying the different horizontal distribution at a different elevation in order to cancel the geometrical acceptance of the system, and compared with the result of Monte Carlo simulations.

The azimuth distributions at different elevations ($\theta = -700, -500, -400, -300, +700, +600, +500, \text{ and } +100 \text{ mrad}$) were normalized to the reference azimuth distribution ($\theta = -600 \text{ mrad}$). Figure 3 shows azimuth distribution of the normalized counts with statistical errors. As can be seen in the figure, the distribution of the backward-directed muons is isotropic within the error bars, but that of the forward-directed muons reflects the local topography. Almost isotropic distribution for $\theta = +100 \text{ mrad}$ is probably the background noise arising from, e.g. vertical showers, which result in fake tracks by hitting two planes almost simultaneously. Therefore, it is very difficult for us to analyze the data for $\theta < +300 \text{ mrad}$. As shown in Fig. 3, a statistically significant excess can be seen at $\phi = +50 \text{ mrad}$. From the topographic information, the muon events will simply decrease as the azimuth angle increases if the density of the target is uniform. This can be systematic error associated to the geometrical efficiency of the segmented detection system. However, such an excess cannot be seen for $\theta \leq -300 \text{ mrad}$ and $\theta = +100 \text{ mrad}$.

Figure 4 shows the derived density length (muon path length times average density along the path line) as a function of angle from horizontal. The estimated density length was compared with the actual path length as measured with the topographic map, assuming a uniform average density to find the lower density region. The lines in Fig. 4 show the thickness of the target, as obtained from the position and the resolution of the apparatus, and the local topography around the fault zone. The uniform density of 2.0 g cm^{-3} was assumed. Overall, there is an agreement between the muon

Interpreting muon radiographic data in a fault zone

H. K. M. Tanaka and
H. Muraoka

[Title Page](#)[Abstract](#)[Introduction](#)[Conclusions](#)[References](#)[Tables](#)[Figures](#)[Back](#)[Close](#)[Full Screen / Esc](#)[Printer-friendly Version](#)[Interactive Discussion](#)

Interpreting muon radiographic data in a fault zone

H. K. M. Tanaka and
H. Muraoka

Title Page

Abstract

Introduction

Conclusions

References

Tables

Figures

⏪

⏩

◀

▶

Back

Close

Full Screen / Esc

Printer-friendly Version

Interactive Discussion

transmission rate and the local topography. By comparing the estimated density length with the actual path length, the average density along the path line can be calculated as shown in Fig. 5, where it is plotted in g cm^{-3} against the horizontal distance from the gauge. Statistically well determined three data points at $\phi = -50, 50,$ and 150 mrad in Fig. 4 were used to draw Fig. 5. As shown in Fig. 3, since the number of fake track N_{BG} is the same order of magnitude as true muon tracks for $\theta < 400$ mrad, the statistical error on the values for these angular regions is seriously masked by the noise.

In Fig. 5, the azimuth angle was converted to the horizontal distance at a distance of 100 m from the detector, representing the middle point of the target whose thickness is ~ 200 m above 300 mrad. It was assumed that the width of the clay gauge (60 cm that is not resolvable with the present detector) is constant throughout the strata. The actual density of 2.2 g cm^{-3} was taken as the density of the clay gauge. In this figure, the density values at ± 5 m are identical for every elevation angles because both values were taken from the data at $\phi = 50$ mrad. It should be noticed that the density values at ± 5 m include the density of the clay gauge, but its contribution is negligible.

4 Results and discussion

Given that the data point at $\phi = 50$ mrad in Fig. 4 must, by the detector orientation, pass through the fault gauge (or the narrow fine-grained core), we see that systematic decrease in the density length (or the average density along the muon path in Fig. 5) from the assumed initial density length (or the average density) around the fault gauge. The center of the fracture zone, due to its high clay content and fine gouge grain size, has high density in general. However, we do not see such a high density in Fig. 5. This is because the resolution of the detector is much lower to capture the gauge width, and thus the density was averaged over a larger spatial extent. However, we can assume that the contribution from the clay gauge to the average density is small.

We also can see that farther away from the fault gauge, density increases. This is because grain damage decreases as a function of the distance from the fault core. The

Interpreting muon radiographic data in a fault zone

H. K. M. Tanaka and
H. Muraoka

Title Page

Abstract

Introduction

Conclusions

References

Tables

Figures



Back

Close

Full Screen / Esc

Printer-friendly Version

Interactive Discussion

5 damage zone half-width, as indicated by the density profiles is ~ 10 m. For reference, a fault zone half width of 10–25 m for the Nojima fault was suggested by Lockner et al. (2009). The result shows that the technique can be applied to monitoring the process of sealing and restrengthening of the seismic fault. It has to be stressed that dynamic muon radiography may provide a good opportunity to monitor how rapidly the enhanced fault zone porous structure will be reduced by sealing and crack healing processes.

10 Most geothermal reservoirs consist of fractures including faults, where permeability is a key factor for estimating the potentials of the hydrothermal convection. The permeability of fractures is theoretically and empirically a function of the porosity as well as porosity-induced density of fracture-filling rocks. The density recovery pattern as a function of the distance from the fault axis demonstrates that muon radiography can be one of the most powerful exploration techniques that directly delineate the permeability structure of the fault zones in detail (Fig. 5).

15 Drilling cost of each geothermal well is estimated in the range of 2–20 million US dollars (Tester et al., 2006) and occupies main part of geothermal exploitations. Nevertheless, available major exploration methods to determine a target fracture by imaging subsurface geothermal reservoirs until the present are only confined to the resistivity and seismic surveys, where they use electromagnetic and elastic waves, respectively, both of which do not go straight on. The positioning resolutions of imaging by these 20 methods are not so satisfactory that the drilling of exploration wells in greenfield areas is reported to have a success rate of typically about 50 to 60 % (Goldstein et al., 2011). About a half of the drilling cost is wasted.

25 Even in a single fault segment, one part acts as a recharge zone and the other part acts as a discharge zone depending on the position of geothermal heat sources and piezometric gradient induced by topography along the fault segment. The dynamic muon radiography by Tanaka et al. (2011) and this paper provide a new method to delineate both the recharge and discharge zones along the fault segment, an entire hydrothermal circulation system. Dynamic muon radiography also provides insights on the flow directions of hydrothermal systems where fluid flow is prevailing along the

Interpreting muon radiographic data in a fault zone

H. K. M. Tanaka and
H. Muraoka

Title Page

Abstract

Introduction

Conclusions

References

Tables

Figures

⏪

⏩

◀

▶

Back

Close

Full Screen / Esc

Printer-friendly Version

Interactive Discussion

- Monograph, Vol. 113, edited by: Haneberg, W. C., Mozley, P. S., Moore, J. C., and Goodwin, L. B., Am. Geophys. Union, Washington, D.C 1999, 101–127, 1999.
- Goldstein, B., Hiriart, G., Bertani, R., Bromley, C., Gutiérrez-Negrín, L., Huenges, E., Muraoka, H., Ragnarsson, A., Tester, J., and Zui, V.: Geothermal Energy, in: IPCC Special Report on Renewable Energy Sources and Climate Change Mitigation, edited by: Edenhofer, O., Pichs-Madruga, R., Sokona, Y., Seyboth, K., Matschoss, P., Kadner, S., Zwickel, T., Eickemeier, P., Hansen, G., Schlömer, S., and von Stechow, C., Cambridge University Press, Cambridge, United Kingdom and New York, NY, USA, 2011.
- Kudryavtseva, V. A., Spoonera, N. J. C., Gluyasb, J., Funga, C., and Coleman, M.: Monitoringsubsurface CO₂ emplacement and security of storage using muontomography, Int. J. Greenh. Gas Con., 11, 21–24, 2012.
- Lockner, D. A. and Byerlee, J. D.: Changes in complex resistivity during creep in granite, Pure Appl. Geophys., 124, 659–676, 1986.
- Lockner, D. A., Tanaka, H., Ito, H., Ikeda, R., Omura, K., and Naka, H.: Geometry of the Nojima fault at Nojima-Hirabayashi, Japan – I. A simple damage structure inferred from borehole core permeability, Pure Appl. Geophys., 166, 1649–1667, 2009.
- Li, Y.-G. and Leary, P.: Fault zone seismic trapped waves, Bull. Seismol. Soc. Am. 80, 1245–1271, 1990.
- Taira, H. and Tanaka, H. K. M.: A potential space-and power-effectivr muon sensor module for imaging a volcano, Earth Planets Space, 62, 179–186, 2010.
- Tanaka, H. K. M.: Evaluation of positioning and density profiling accuracy of muon radiography by utilizing a 15-ton steel block, Geosci. Instrum. Method. Data Syst. Discuss., 2, 643–656, doi:10.5194/gid-2-643-2012, 2012.
- Tanaka, H. K. M. and Sannomiya, A.: Development and operation of a muon detection system under extremely high humidity environment for monitoring underground water table, Geosci. Instrum. Method. Data Syst. Discuss., 2, 719–736, doi:10.5194/gid-2-719-2012, 2012.
- Tanaka, H. K. M., Uchida, T., Tanaka, M., Takeo, M., Oikawa, J., Ohminato, T., Aoki, Y., Koyama, E., and Tsuji H.: Detecting a mass change inside a volcano by cosmic-ray muon radiography (muography): First results from measurements at Asama volcano, Japan, Geophys. Res. Lett., 36, L17302, doi:10.1029/2009GL039448, 2009.
- Tanaka, H. K. M., Miyajima, H., Kusagaya, T., Taketa, A., Uchida, T., and Tanaka, M.: Cosmic muon imaging of hidden seismic fault zones: Rainwater permeation into the mechanical

fractured zones in Itoigawa-Shizuoka Tectonic Line, Japan, Earth Planetary Sci., 306, 156–162, 2011.

5 Tester, J. W., Anderson, B. J., Batchelor, A. S., Blackwell, D. D., DiPippo, R., Drake, E. M., Garnish, J., Livesay, B., Moore, M. C., Nichols, K., Petty, S., Toksöks, M. N., and Veatch Jr., R. W.:
The Future of Geothermal Energy: Impact of Enhanced Geothermal Systems on the United States in the 21st Century, Prepared by the Massachusetts Institute of Technology, under Idaho National Laboratory Subcontract No. 63 00019 for the US Department of Energy, Assistant Secretary for Energy Efficiency and Renewable Energy, Office of Geothermal Technologies, Washington, DC, USA, 358 (ISBN-10: 0486477711, ISBN-13: 978-0486477718),
10 available at: geothermal.inel.gov/publications/future_of_geothermal_energy.pdf, 2006.

GID

2, 875–891, 2012

Interpreting muon radiographic data in a fault zone

H. K. M. Tanaka and
H. Muraoka

Title Page

Abstract

Introduction

Conclusions

References

Tables

Figures

◀

▶

◀

▶

Back

Close

Full Screen / Esc

Printer-friendly Version

Interactive Discussion

Interpreting muon radiographic data in a fault zone

H. K. M. Tanaka and
H. Muraoka

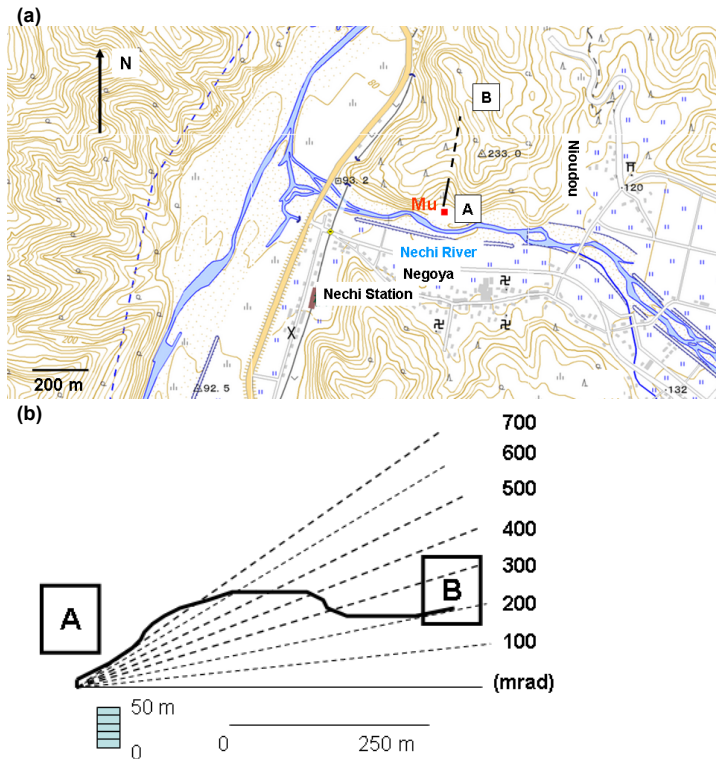


Fig. 1. Geometrical arrangement for the detection system versus Itoigawa Shizuoka Tectonic Line (ISTL) fault line taken in the present measurement. A topographic map indicating the detector location Mu (a) and a cross sectional view of the topography along A-B line ($\phi = 0$ mrad) are shown. The discovered fault line and the estimated fault line are indicated by a solid and broken line in (a).

Title Page

Abstract Introduction

Conclusions References

Tables Figures

◀ ▶

◀ ▶

Back Close

Full Screen / Esc

Printer-friendly Version

Interactive Discussion

Interpreting muon radiographic data in a fault zone

H. K. M. Tanaka and
H. Muraoka

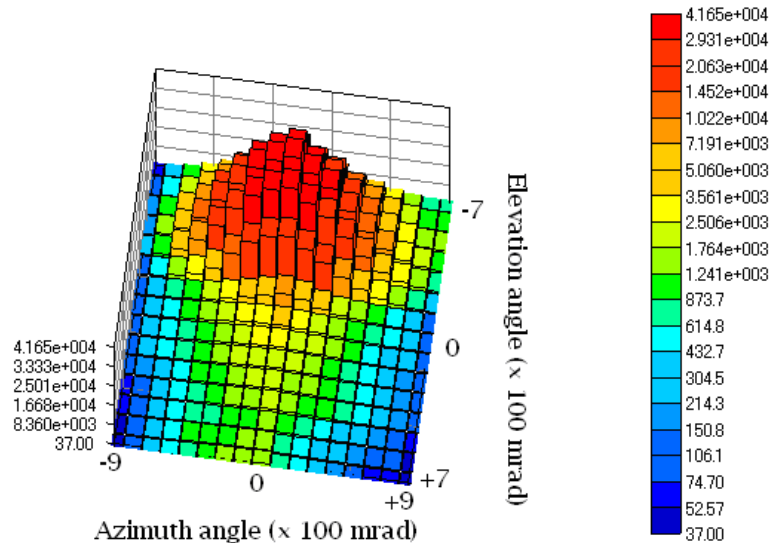


Fig. 2. Histogram of the muon events collected in the present experiment. Horizontal and vertical bin width is 100×100 mrad with the root mean square angular resolution is ± 40 mrad. The positive (and negative) elevation angles refer to the “forward-directed” (and “backward-directed”) muon events.

[Title Page](#)
[Abstract](#)
[Introduction](#)
[Conclusions](#)
[References](#)
[Tables](#)
[Figures](#)
[⏪](#)
[⏩](#)
[◀](#)
[▶](#)
[Back](#)
[Close](#)
[Full Screen / Esc](#)
[Printer-friendly Version](#)
[Interactive Discussion](#)

Interpreting muon radiographic data in a fault zone

H. K. M. Tanaka and
H. Muraoka

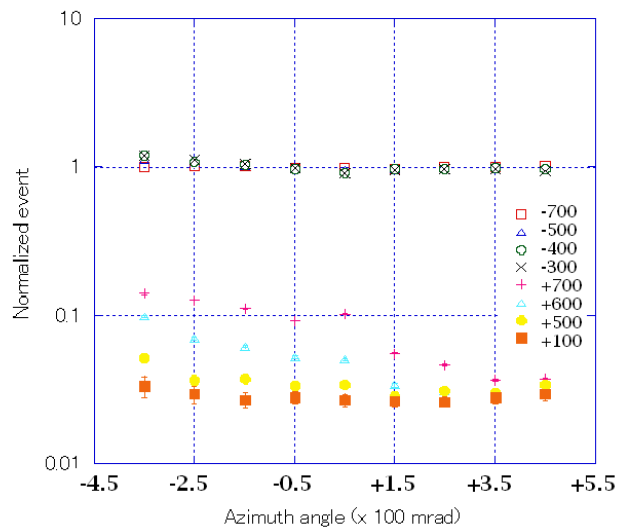


Fig. 3. Azimuth distributions at different elevations ($\theta = -700, -500, -400, -300, +700, +600, +500,$ and $+100$ mrad) normalized to the reference azimuth distribution ($\theta = -600$ mrad).

Title Page

Abstract

Introduction

Conclusions

References

Tables

Figures



Back

Close

Full Screen / Esc

Printer-friendly Version

Interactive Discussion

Interpreting muon radiographic data in a fault zone

H. K. M. Tanaka and
H. Muraoka

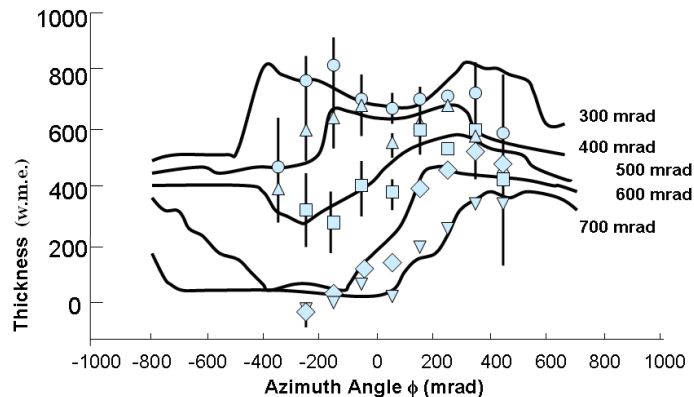


Fig. 4. Elevation dependence of the density length as a function of azimuth angle. The solid lines show the density lengths as measured from the topographic map by assuming a uniform density of 2.0 g cm^{-3} . The measurements and the related error bars can be referred to the scale and unit on the vertical axis. The bottom axes indicate the azimuth angles (ϕ in units of mrad) with reference to the line perpendicular to the detector plane and path lengths respectively.

[Title Page](#)
[Abstract](#)
[Introduction](#)
[Conclusions](#)
[References](#)
[Tables](#)
[Figures](#)
[⏪](#)
[⏩](#)
[◀](#)
[▶](#)
[Back](#)
[Close](#)
[Full Screen / Esc](#)
[Printer-friendly Version](#)
[Interactive Discussion](#)

Interpreting muon radiographic data in a fault zone

H. K. M. Tanaka and
H. Muraoka

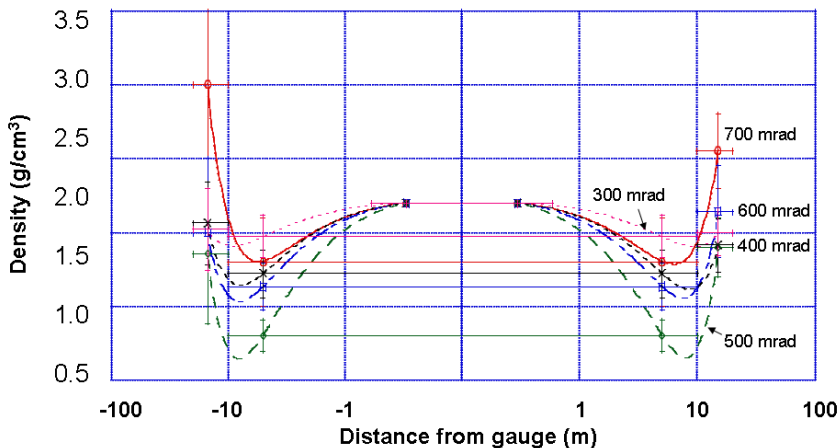


Fig. 5. Density distribution as a function of the distance from the fault gauge. The vertical error bar shows the statistical error, and the horizontal error bar indicates the positioning resolution of the detector. The data points are fitted to guide the eye for visible convenience.

[Title Page](#)[Abstract](#)[Introduction](#)[Conclusions](#)[References](#)[Tables](#)[Figures](#)[⏪](#)[⏩](#)[◀](#)[▶](#)[Back](#)[Close](#)[Full Screen / Esc](#)[Printer-friendly Version](#)[Interactive Discussion](#)

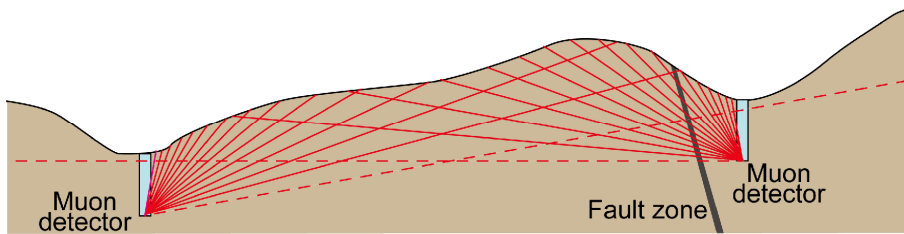


Fig. 6. Scheme of the down-hole muon radiography.

Interpreting muon radiographic data in a fault zone

H. K. M. Tanaka and
H. Muraoka

[Title Page](#)

[Abstract](#) [Introduction](#)

[Conclusions](#) [References](#)

[Tables](#) [Figures](#)

[⏪](#) [⏩](#)

[◀](#) [▶](#)

[Back](#) [Close](#)

[Full Screen / Esc](#)

[Printer-friendly Version](#)

[Interactive Discussion](#)

